An Acad Bras Cienc (2024) 96(4): e20240365 DOI 10.1590/0001-3765202420240365
Anais da Academia Brasileira de Ciências | *Annals of the Brazilian Academy of Sciences*
Printed ISSN 0001-3765 I Online ISSN 1678-2690
www.scielo.br/aabc | www.fb.com/aabcjournal

GEOSCIENCES

Petrographic and Petrophysical Characterization of Sandstones from Rio Bonito Formation, Paraná Basin (Southern Brazil)

PAULO FREDERICO O. RAMOS, GIOVANNI C. STAEL, RODRIGO B.V. AZEREDO, MARCUS VINICIUS B. ADE, SÉRGIO BERGAMASCHI, JUAREZ LOURENÇO & SILVIA LORENA B. BERMUDEZ

Abstract: This study focuses on the laboratory-scale petrophysical characterization of sandstones from the Rio Bonito Formation (Lower Permian), Paraná Basin, carried out from drill core samples from well PN-14-SC.02 obtained by CPRM-Brazilian Geological Service in the 1980s on the eastern edge of the Basin. This study includes integrating experimental data from routine petrophysics, sedimentary petrography, and nuclear magnetic resonance (NMR) obtained from 6 samples arranged in the normal direction of the stratification, present between 40 and 200 m deep. It was possible to conclude that the values of the permeability and porosity properties obtained from the NMR technique correlated in a very satisfactory way, with correlation coefficient R^2 = 0.957 and Root Mean Squared Error (RMSE) = 0.208 about the porosity reference results offered by routine petrophysics, with lower values being less than a porosity unit (+/- 1 p.u.), in the range between 8 and 14%. The same was observed for the estimated permeability, R^2 = 0.885 and RMSE = 0.152, by the Timur Coates method, with values in the range between 0.096 and 2.42 mD, which were well supported by the spectra information, as well as by petrographic analyses.

Key words: Permeability, Porosity, Nuclear Magnetic Resonance, Rio Bonito Formation, Parana Basin.

INTRODUCTION

The characterization of reservoirs plays a crucial role in oil exploration and exploitation. The scenario exposed at present is an increase in production costs and difficulty in accessing the reservoirs of interest. In addition, the different types, internal organization, and diagenetic effects on the permeability and porosity properties of siliciclastic reservoirs are significant and active in the characterization of these reservoirs Schmidt & McDonald (1979), Giles & Marshall (1986), Giles & De Boer (1989). The study of petrophysical properties, such as porosity and permeability, is fundamental for understanding the mechanisms that impact production, allowing a more realistic evaluation of the strategies to be chosen aimed at the economic development of the studied reservoirs.

Thus, the Rio Bonito Formation in the Paraná Basin was chosen due to its relationship with coastal and marine sandstone deposits that are traditionally considered suitable hydrocarbon reservoirs due to their permeability and porosity characteristics, as well as a good analog for studies of these physical attributes of the rock. Sandstone samples from well PN-14-SC.02 of the Rio Bonito Formation were used in this study because, although there are studies that emphasize the properties of this formation

Milani et al. (1990), Ketzer et al. (2003), Bocardi et al. (2009), Silva (2011), little or no characterization of the physical attributes of the rocks and their saturating fluids was observed. These previous studies interpreted the sequence of diagenetic activities and the relative importance of these processes in reducing porosity. The motivation for the present study is the lack of studies involving the laboratory petrophysical evaluation of the Rio Bonito Formation, in particular, using the application of different characterization methodologies from the integration of porosity, permeability and grain density data, which are obtained by routine petrophysical techniques Tiab & Donaldson (2004), petrography and NMR Kleinberg & Jackson (2001) so that the characteristics of the rocks can be known and determined in a rapid and accurate analysis, providing a better understanding of the permeability and porosity properties of reservoirs and their production potential.

GEOLOGICAL SETTINGS

The studied well, drilled on the eastern edge of the Paraná Basin in the State of Santa Catarina, southern Brazil (Figure 1), entirely crosses the Rio Bonito Formation (Lower Permian), recovering a cyclic succession of sediments of sandstones, siltstones, and shales, in addition to intervals of coal deposits of this unit.

A narrow band in the Brazilian states of São Paulo (SP), Santa Catarina (SC), Paraná (PR), and Rio Grande do Sul (RS), extending into Uruguay. The tectono-sedimentary history of the Gondwana succession of the Paraná Basin begins with Carboniferous subsidence and the deposition of the Aquidauana-Itararé units. Overlapping the Itararé Group are sandstones, siltstones, and coalbeds of the Rio Bonito Formation Bocardi et al. (2009). The deposition of the Rio Bonito Formation occurred in paleovalleys excavated by the glaciers that preceded them, and the subsidence was later influenced by the weight of the sediments deposited throughout the transgressive-regressive cycle Medeiros & Thomas (1973), Zalán et al. (1987). The coastal and marine deposits related to the Rio Bonito Formation are considered suitable reservoirs; however, the controls for the heterogeneity of these reservoirs are poorly understood. The Paraná Basin has extensive reserves of natural and mineral resources that have been researched and explored for some time. Previous studies have also shown that source rocks occur in some stratigraphic units, including the Ponta Grossa Formation, Irati Formation, and Rio Bonito Zalán et al. (1987).

At the basin's eastern edge, the Rio Bonito Formation is subdivided into three units (Figure 2) named from the bottom up as the Triunfo, Paraguaçu, and Siderópolis Members Schneider et al. (1974).

Bocardi et al. (2009) studied and interpreted the sequence of the diagenetic processes that acted on the sandstones that constitute the Rio Bonito Formation and the relative importance of the compaction and cementation processes in the reduction in porosity using thin sections and well data (controls and gamma-ray log). The clay minerals were analyzed by X-ray diffraction, and the relationships between the minerals were evaluated using scanning electron microscopy.

The porosity characteristics of the reservoir rocks, in the range of 20%, indicate that the coastal and marine deposits of the Rio Bonito Formation can be considered suitable reservoirs Milani & Zalán (2000), even at great burial depths, which would make them good analogs for studies of existing deposits.

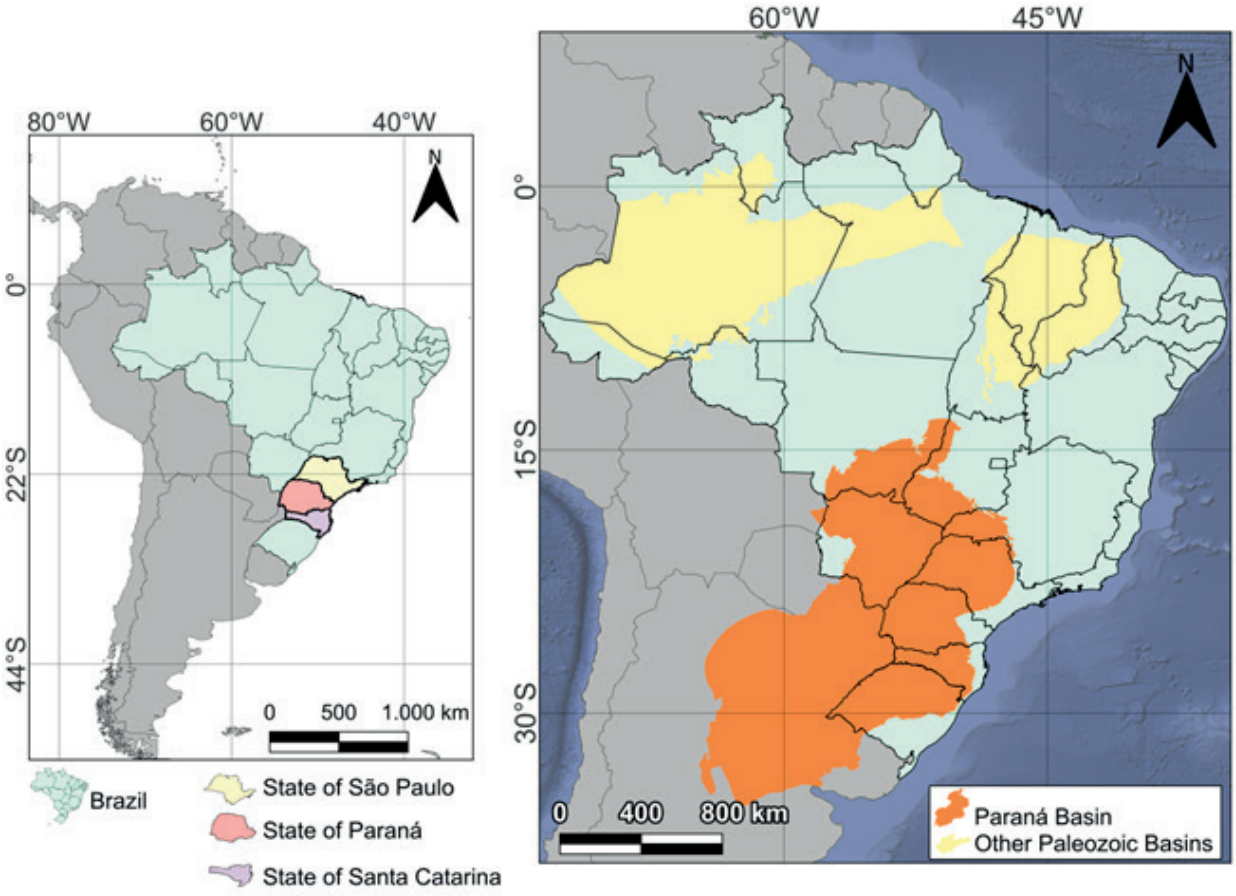

Figure 1. Location of the Paraná Basin (modified from Casagrande 2010).

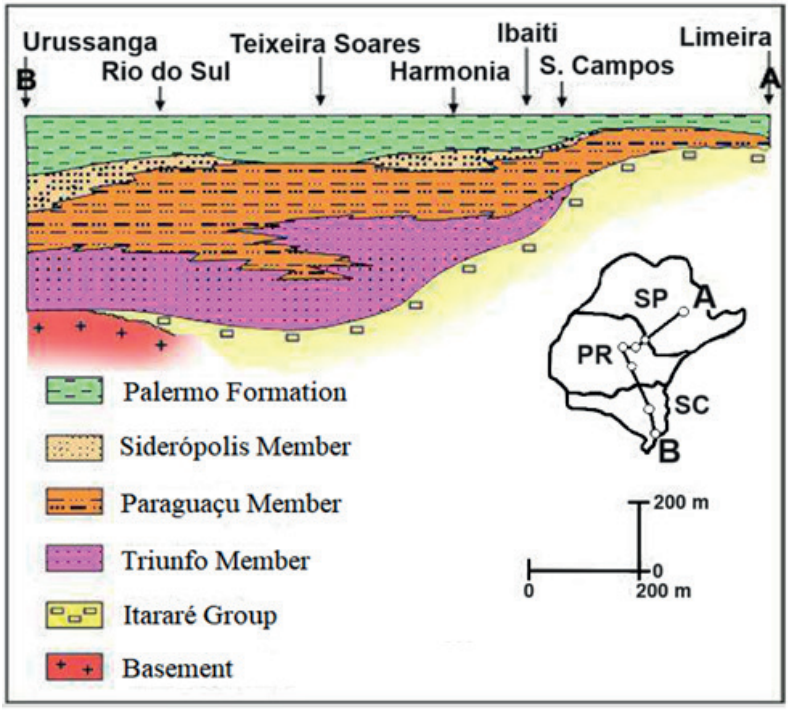

Figure 2. Distribution of the Triunfo, Paraguaçu and Siderópolis Members of the Rio Bonito Formation in the states of Santa Catarina (SC), Paraná (PR), and São Paulo (SP) (modified from Schneider et al. 1974).

MATERIALS AND METHODS

Six samples were selected from drill cores from well PN-14-SC.02 of the Rio Bonito Formation, between depths of 40 and 200 m, drilled by DNPM/CPRM in the 1980s on the eastern edge of the Paraná Basin, more specifically in the municipality of Alfredo Wagner, State of Santa Catarina Santa Catarina (SC) (Figure 3).

These cores were sent to the Petrophysics Laboratory of the National Observatory (LabPetrON), Rio de Janeiro, Brazil, for petrophysical analyses. The samples were prepared to meet the specific needs of the analytical techniques.

Petrography

The next stage was the preparation of petrographic thin sections at the Department of Geology of the Federal University of Rio de Janeiro-UFRJ and subsequent analysis at the School of Geology of the University of the State of Rio de Janeiro-UERJ. The petrographic analysis aimed to evaluate the influence of morphology and/or texture, mineralogy, and diagenetic processes on the permeability and porosity characteristics of the studied rocks.

The sandstone samples were impregnated with blue epoxy to identify the pores and fix the mineral grains. The samples were analyzed and photographed using a ZEISS binocular optical microscope. Photomicrographs were obtained with parallel and crossed nicols (polarized), with magnification between 100x and 400x.

In this stage, we sought to establish a correlation between the petrographic analysis and the data generated in the routine petrophysical characterization.

Routine Petrography

The initial step was to prepare the samples in the form of plugs 2.54 cm (1") in diameter and height by cutting the cores in the orthogonal

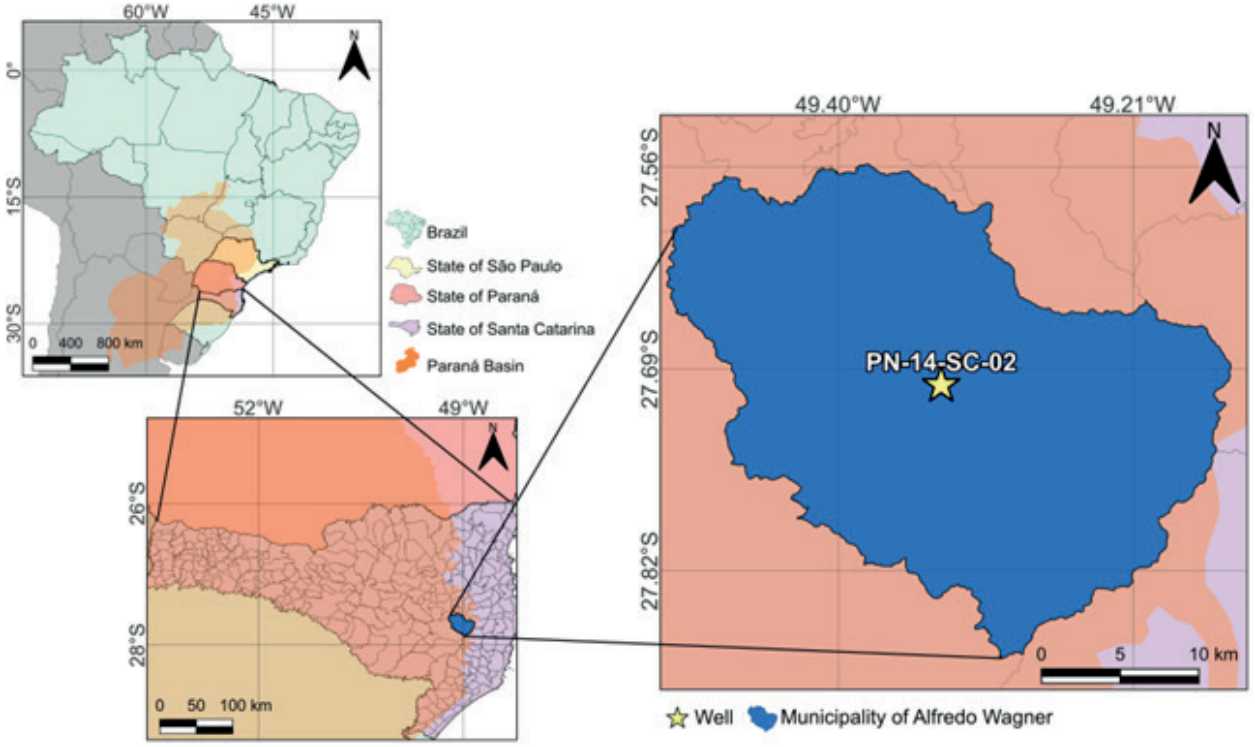

Figure 3. The location of the PN-14-SC.02 well is in the municipality of Alfredo Wagner in the state of Santa Catarina (modified from Casagrande 2010).

(vertical) direction to stratification in cutting machines belonging to LabPetrON according to the procedures recommended by the American Petroleum Institute (1998).

After preparation, the routine petrophysical properties were directly characterized and used as references. The tests were performed with a confining pressure (hydrostatic) of 500 psi at Core Laboratories (USA) equipment: Ultraperm 500 for measurement of absolute permeability, according to Darcy's law, and Ultrapore 300 for measurement of effective porosity, solids volume, and grain density, according to Boyle's law, both using nitrogen. The tests were conducted at a room temperature of 22 °C and an average relative humidity of 50%.

Nuclear Magnetic Resonance (NMR)

For the NMR analyses, the plugs were saturated entirely with NaCl solution and equivalent salinity (50,000 ppm) under the application of vacuum and positive pressure in the samples of low permeability (k_{abs} < 200 mD). The plugs were submerged in saline solution until the NMR assays were performed.

A benchtop Maran Ultra 2 MHz NMR spectrometer (Oxford Instruments, UK) was used with a magnetic field (B_0) of 460 Gauss, equivalent to a frequency of 2 MHz for 1 H, existing at LabPetrON.

The raw data of the transversal relaxation time (T_2) were obtained using the Carr–Purcell–Meiboom–Gill (CPMG) pulse sequence Meiboom & Gill (1958), and the processing software was WinDXP. The parameters used are summarized in Table I.

RESULTS AND DISCUSSIONS

In this chapter, a comparative investigation is performed between the results obtained by the analytical methods of petrography, routine petrophysics, and nuclear magnetic resonance, aiming at a better understanding of the permeability and porosity properties of the samples. The names and depths of the samples are presented below in the petrographic analyzes.

Petrography Analysis

The petrographic analysis performed in this study aimed to evaluate the morphological and/or textural influence of the porous system, the mineralogy, and the diagenetic processes of the studied samples to support the results obtained by the other techniques mentioned.

Table I. Main parameters of NMR acquisition.

Main Acquisition Parameters	
Temperature	35 °C
Number of echoes	8192
Lag time	200 µs
Repetition time	10 s
P90	10.5 µs
P180	20.3 µs
Receiver gain	100%
Signal-to-noise ratio	100

In the sandstone sheets, predominantly grains of quartz, feldspar, and, subordinately, muscovite were observed. According to the classification by Folk (1968), these sandstones were classified as quartz sandstones and subarkoses Dott (1964), Folk (1968).

Sample BV1 and BV2 (Depth of 50.20 m)

Many interconnected pores were observed (Figure 4) in thin sections of photomicrograph 4. b, mainly in the quartz sandstone. In addition to quartz, grains of K-feldspar, micas (muscovite and biotite), plagioclases, and clay minerals such as kaolinite and illite were observed, the clay minerals occurring as pore-filling cement (authigenic minerals). Petrographically, the grains are fine, subrounded to rounded, and a certain degree of compaction is observed, suggesting that they were buried at moderate depths.

The porosity presented is secondary mainly due to the processes involved, such as compression by pressure, observing the syntaxial growth of quartz, with fringes around the original grain, and authigenic kaolinite cement, resulting from the feldspar replacement and pore filling. The microporosity is not observed by the presence of kaolinite, among other clay minerals, which "mask" this porosity in the field of view.

Sample EH3 (Depth of 52.40 m)

This sample presents subarkosic rock, with moderate gradual selection, fine grains, fractures, evidence of compaction, concave-convex, straight and (fewer) sutured contacts (Figure 5). The grains are subrounded with low sphericity. Among the main constituents are the grains of quartz, K-feldspar, plagioclase, muscovite, and opaque minerals. Pyrite and clay minerals such as kaolinite were observed among the diagenetic constituents. The secondary porosity is well evidenced by the heterogeneity in the pore size, dissolved grains, floating grains, partially corroded grains, and enlarged pore throats. Isolated pores were also found, highlighting the secondary porosity, such as intergranular and moldic pores. Diagenesis is the primary factor in forming secondary porosity, especially the chemical dissolution of feldspar and, secondarily, quartz.

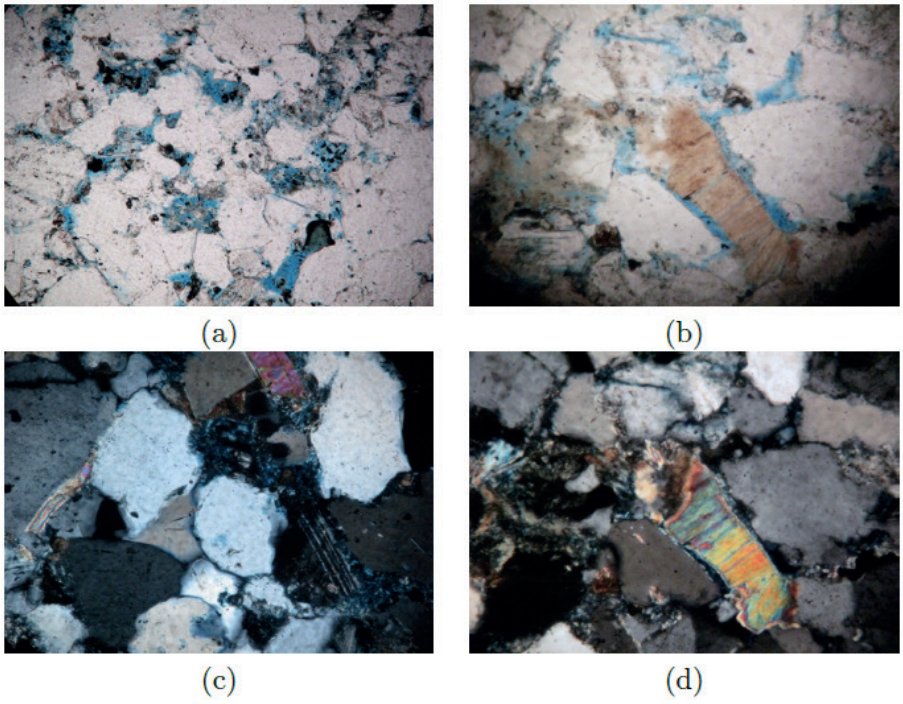

Figure 4. (4.a) and (4.b) Photomicrographs with parallel nicols at 20x magnification. (4.c) Moreover, (4.d) Photomicrographs with crossed nicols (polarized light), with 40x magnification. The porosities observed are secondary, intergranular, and moldic.

As diagenetic processes, the pressure dissolution of quartz, syntaxial growth of quartz, pore filling by calcite cement, pore filling by clay minerals (especially kaolinite), and precipitation of iron oxide hydroxides deserve to be highlighted.

Sample FH1 (Depth of 58.98 m)

Sample FH1 is characterized as a fine- to medium-grained white, kaolinic sandstone, with moderate to good grading and subrounded to rounded grains, moderate porosity, and cross bedding, with dark clay films in the bedding planes. This sample can be characterized as subarkosic. Quartz grains, K-feldspar, plagioclase, muscovite, and opaque minerals predominate in its framework. The presence of isolated pores was verified. The secondary porosity was intergranular and intragranular (Figure 6 - photomicrographs 6.c and 6.d) and, subordinately, moldic. Calcite carbonate cement and quartz syntaxial growth were found (photomicrographs 6.a and 6.b). Carbonate and feldspar dissolution was also observed in the thin sections.

Sample HVI (Depth of 157.70 m)

Sample HV1 (Figure 7) consists of fine- to medium-grained white kaolin sandstone with moderate grading and subrounded grains. The porosity is moderate to low, and the bedding angle is low. The thin section observed is of quartz sandstone. Quartz, K-feldspar, muscovite, plagioclase, and opaque minerals predominate among the grains. Concave-convex and planar contacts predominate, with punctual and sutured contacts observed. Secondary porosity due to grain and cement dissolution and fracturing is also observed, predominantly of the intergranular and moldic types. In the diagenetic processes evidenced, the chemical dissolution of feldspathic grains, syntaxial growth of quartz (photomicrographs 7.b and 7.d), presence of carbonate cement and authigenic kaolinite (photomicrographs 7.a and 7.b) were observed.

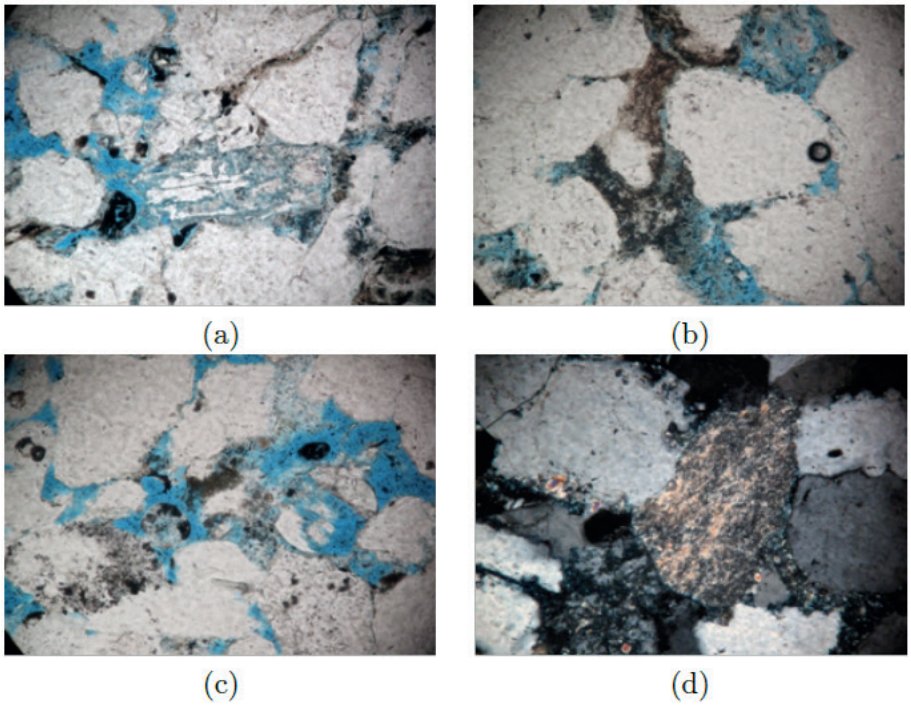

Figure 5. (5.a), (5.b) and (5.c) Photomicrographs at 20x, 40x, and 20x magnification, respectively, obtained with parallel nicols, with emphasis on porosity, with essential participation of secondary porosity. (5.d) Photomicrographs showing, at the center of the image, a grain of illite, obtained with polarized light (crossed nicols) and 40x magnification.

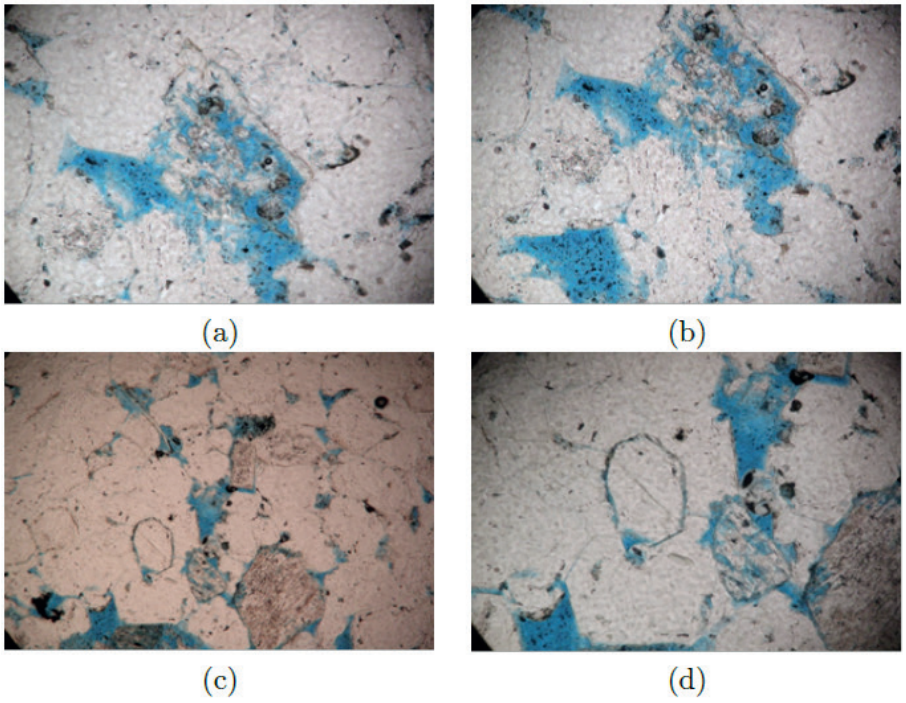

Figure 6. (6.a), (6.b), (6.c) and (6.d) Photomicrographs with parallel nicols. Magnification of 20x, 20x 10x and 20x. The porosities observed are secondary, intragranular, intergranular, and moldic.

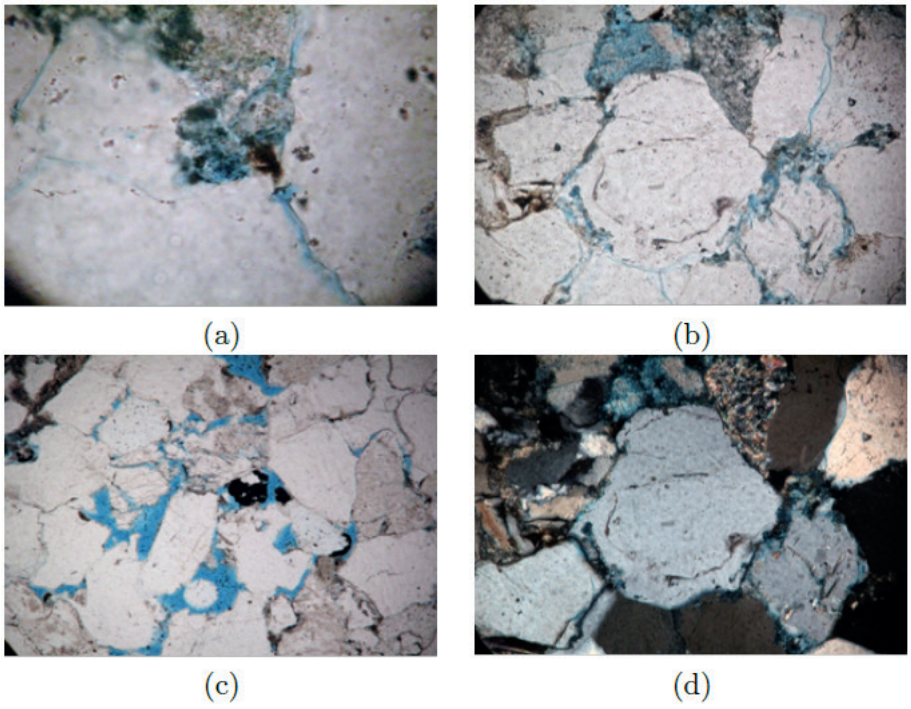

Figure 7. (7.a), (7.b), (7.c) and (7.d) Photomicrographs at 50x, 40x, 20x and 40x magnification, respectively, using parallel nicols in the first three and polarized light (crossed nicols) in the last.

Sample JVI (Depth of 193.77 m)

Sample JV1 (Figure 8) is a fine, white kaolin sandstone, with moderate to good grading. Its grains are subrounded to rounded, its porosity is moderate to low, and its sedimentary structure has low angle bedding. It is possible to observe the presence of kaolinite derived from the dissolution of feldspar. In addition to the quartz grains, grains of K-feldspar, muscovite (photomicrographs 8.a and 8.b), plagioclase,

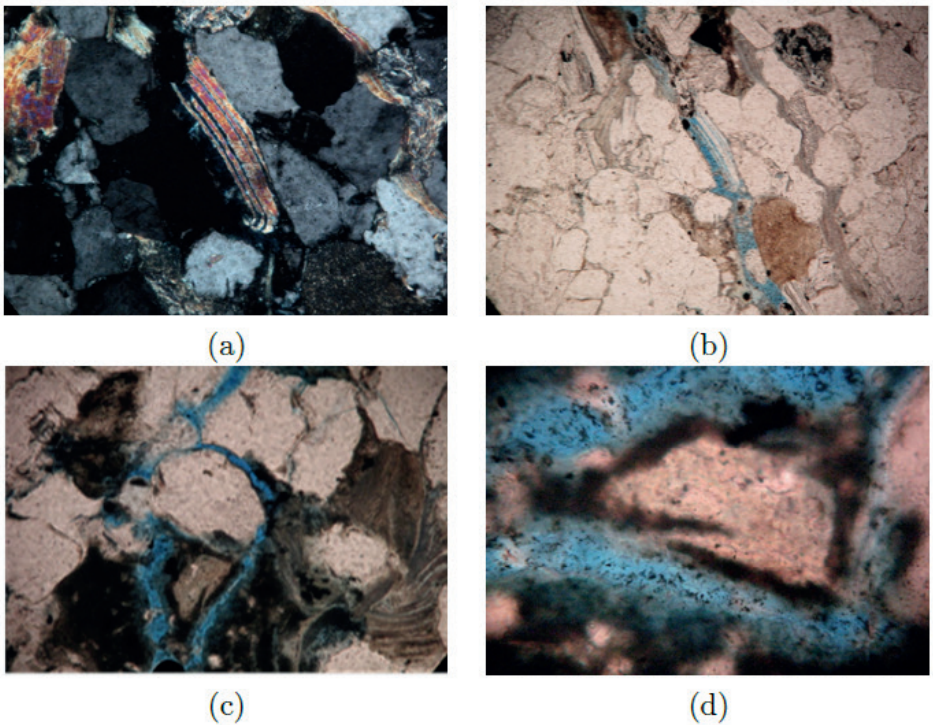

Figure 8. (8.a) and (8.b) Photomicrographs at 20x and 50x magnification, crossed nicols and parallel. Secondary, intergranular, moldy, and canal porosities can be observed in (8.b), (8.c), and (8.d).

biotite, and opaque minerals were found. Among the cement, the syntaxial growth of quartz, calcium carbonate, kaolinite, and illite stands out, as well as precipitates of iron oxide-hydroxide. The predominant porosity is secondary intergranular. The most remarkable diagenetic processes are the chemical dissolution of grains such as feldspar and the syntaxial growth of quartz (fringing). The presence of authigenic clayey cement was observed (photomicrographs 8.c and 8.d) in the pore space, noting that the kaolinite includes the microporosity between the largest grains. Photomicrograph 8.d shows this aspect of photomicrograph 8.c in detail. The presence of clay from mechanical infiltration is evident. Secondary, intergranular, moldy, and canal porosities can be observed in Photomicrographs 8.b, 8.c, and 8.d.

Analyses of the Routine Petrophysical Properties

The analyses of the routine petrophysical properties, such as effective porosity and absolute permeability, were performed by direct measurement in the longitudinal direction of the samples, orthogonal to the bedding. The results are summarized in Table II below.

The low permeabilities and reasonable porosity found in the routine analysis, closely corresponded to the textures observed in the petrographic thin sections, which are formed predominantly in the fine- to medium-grained sandstones due to high clay contents in the porous system.

Nuclear Magnetic Resonance (NMR)

Once characterized by routine petrophysics, standard, or reference methods, the samples were analyzed by nuclear magnetic resonance. This technique consists of the polarization of hydrogen nuclei present in the fluids of the porous system of rocks so that a radiofrequency pulse deflects their magnetization in the direction of the permanent field. Upon returning to the initial conditions, the nuclear magnetic relaxation Gil & Geraldes (1987), Levitt (2001) will produce a signal

characteristic of the structural organization of the analyzed material. Based on this principle, we can estimate porosity and permeability through the signal intensity generated by the volume and the appearance of the fluid distribution within the sample. The results obtained are compared to the reference values.

Total Porosity by NMR

Table III below shows a comparison between the values of routine petrophysics and the results obtained as a function of the NMR analysis. Figure 9 shows a correlation graph between the values of these porosities, the respective correlation coefficients, and their mean deviation.

In comparing the porosity results (Figure 9), there is an average deviation smaller than one porosity unit between the methodologies, producing an excellent linear correlation. Considering the routine data as a reference, the NMR results demonstrate the method's reliability and ensure that the preparation of the samples was performed correctly.

Distribution of Pore Size

In addition to obtaining the porosity by the NMR method, it is possible to estimate the

Table II. Results of routine petrophysical property tests.

Samples	Depth (m)	Pressure (psi)	Total volume (cm^3)	Mass (g)	Volume of solids (cm^3)	Density (g/cm^3)	Porous volume (cm^3)	Porosity (%)	Absolute Permeability (mD)
BV1	50.20	500	13.41	30.32	11.46	2.65	1.87	14.0	2.35
BV2	50.20	500	13.76	31.09	11.69	2.66	1.83	13.5	1.13
EH1	52.40	500	14.00	32.46	12.25	2.65	1.58	11.4	0.363
FH1	58.98	500	18.06	41.21	15.46	2.67	2.44	13.6	2.85
HV1	157.70	500	18.01	41.68	15.71	2.65	2.02	11.4	1.79
JV1	193.80	500	18.06	43.80	16.38	2.67	1.57	8.7	0.096

Table III. Comparative results between routine and NMR porosities.

Samples	Depth (m)	Porosity (%)			
		Routine (N_2)	NMR	R^2	RMSE
BV1	50.2	14.0	13.5	0.957	0.208
BV2	50.2	13.5	13.1		
EH3	52.4	11.3	11.4		
FH1	59.0	13.9	13.7		
HV1	157.7	11.4	11.9		
JV1	193.8	8.7	8.0		

pore size distribution of the samples from the electromagnetic interaction between the rock and the fluid (hydrogen) contained in the pore volume.

Figure 10 shows the decay signals of the brine, in yellow, and the saturated samples. The maximum initial amplitude observed in the curves is a direct expression of the volume of fluid present in the samples Zhang et al. (2000). The rapid decay observed in the curves of the raw T_2 data suggests the predominance of small pores in the samples of the Rio Bonito Formation, corresponding to the low permeabilities recorded by the routine.

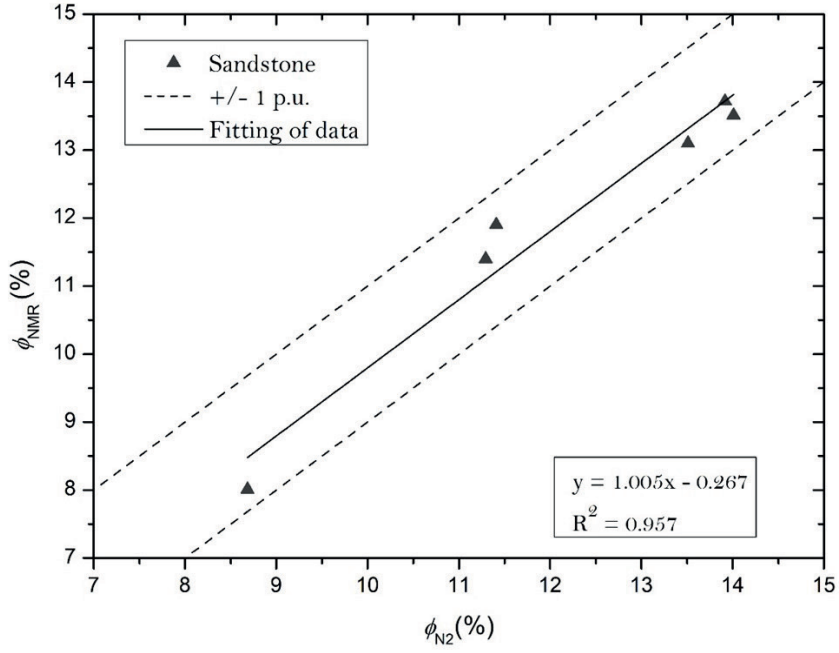

Figure 9. Correlation between the porosity values obtained in the routine analysis (N_2) and by NMR.

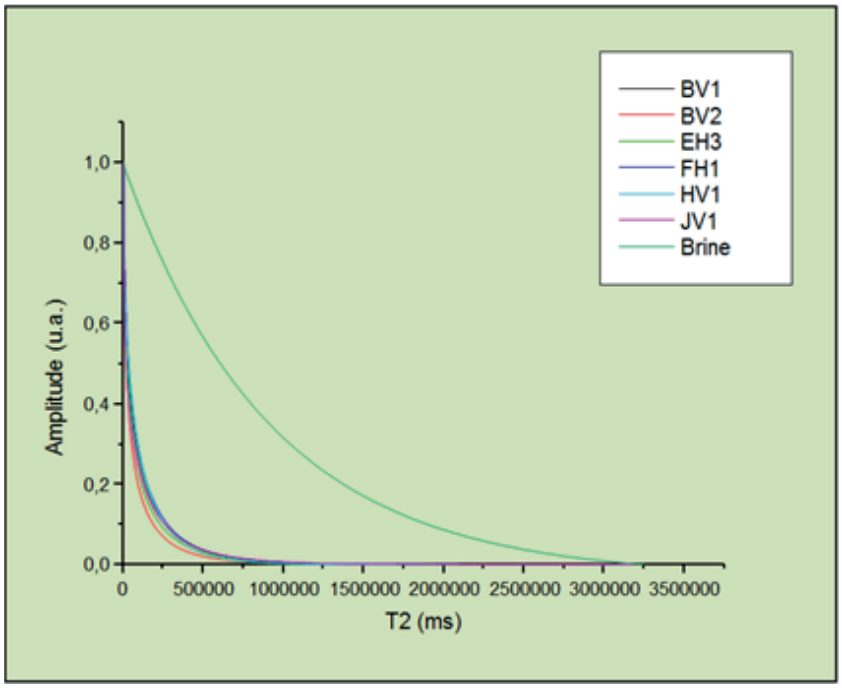

Figure 10. Decay curves of the raw T_2 data of the calibration sample (brine) and the studied rock samples.

Relaxation Spectrum T_2

Figure 11 shows the transverse relaxation spectra (T_2) for the sandstone samples used in this study. Each spectrum, obtained by inversion of the relaxation curves, consists of 128 points logarithmically distributed between 0.1 ms and 10 s. Table IV below shows a correlation between the T_2 relaxation time and the pore sizes of a rock Lowden et al. (1998), Benavente et al. (2001), Cranganu et al. (2009), i.e., a pseudo-pore size distribution via NMR, as classified by mercury injection capillary pressure MICP

Sample BV1

In the studies performed on the BV1 sample (Figure 11 - black line), the bimodal trend was observed with a geometric mean relaxation time (T_{2gm}) of 34.6 ms in the interval between 0.1 and 500 ms, indicating a distribution in the nano- to mesopores, where approximately 80% of the porosity is concentrated up to the mesopore region. These values can indirectly relate to predominantly fine particle size, corroborating the petrographic thin sections' observations (Figure 4).

Sample BV2

In Figure 11 - red line, the BV2 sample also showed a bimodal trend, with a geometric mean relaxation time (T_{2gm}) of 25.0 ms, shorter than that of the BV1 sample, but with a similar relaxation time distribution, covering nano- and mesopores

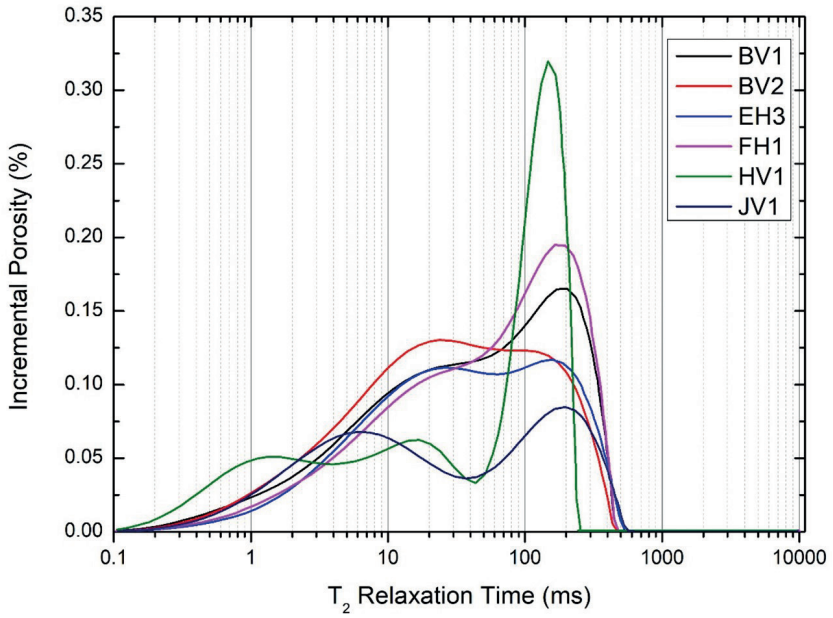

Figure 11. Spectrum of the distribution of transverse relaxation time (T_2) of saline solution contained in the porous system of all the samples.

Table IV. Correlation of pore size and T_2 relaxation time.

Pore size (µm)	T_2 value (ms)
Nano < 0.1	Below 1
Micro 0.1-0.5	1 to 10
Meso 0.5-2	10 to 100
Macro 2-10	100 to 1000
Mega >10	1000 to 10000

in the range of 0.1 to 440 ms, with a higher concentration in the micro- to mesopores region. Similarly, it is possible to relate the relaxation values indirectly to predominantly fine particle size, validating the observations made in the petrographic analyses (Figure 4).

Sample EH3

It was observed that the spectrum of the EH3 sample (Figure 11 - blue line) has a bimodal trend, with a geometric mean relaxation time (T_{2gm}) at 32.3 ms and a spectral distribution ranging between nano- and mesopores in the range 0.1 and 510 ms. The T_{2gm} value was higher than that observed in the BV2 sample, indicating an increase in the concentration of the pore volume in the mesopore region, testifying to the presence of a greater volume of secondary porosity (Figure 5) observed in the thin sections.

Sample FH1

In Figure 11 - pink line, the spectrum of sample FH1 has a bimodal trend, with its geometric mean relaxation time (T_{2gm}) at 42.4 ms and a wide distribution of its spectrum covering a scale between nano- and mesopores in the interval 0.1 and 443 ms. A concentration of the pore volume covers the mesopore region, where the concentration in more extensive logarithmic decades explains the higher porosity of the sample, which reflects its petrography (Figure 6), with apparent secondary porosity, both intergranular and intragranular.

Sample HVI

In the HV1 sample (Figure 11- green line), a trimodal trend was observed in its spectrum, with the geometric mean relaxation time (T_{2gm}) at 26.9 ms and a wide distribution between nano- and mesopores in the 0.1 and 235 ms range. A concentration of the pore volume was observed in the micro- and mesopore range, emphasizing the mesopores. However, a significant area, approximately 25% of the total, is concentrated between nano- and micropores, corroborating the petrographic thin section in the presence of clay minerals and secondary porosity due to fracturing (Figure 7). The observations support the permeability reference values found in routine petrophysics. In this sample, the porosity is defined as the secondary porosity due to intergranular and moldic pores and fractures.

Sample JV1

The JV1 sample (Figure 11- purple line) shows bimodal spectra, with a geometric mean relaxation time (T_{2gm}) of 21.8 ms and the distribution of its spectrum between nano- and mesopores in the range of 0.1 and 531 ms, where a pronounced concentration of the pore volume is observed in the micro- and mesopore regions, indicating a lower porosity, corroborating the observations highlighted in petrographic thin sections (Figure 8), by the presence of clay distributed in a secondary intergranular and moldic porosity.

From the correlation of the T_2 relaxation times and pore sizes (Table IV), it was possible to generate a radar graph (Figure 12) of the pore size distributions of the analyzed samples and verify that the areas of the polygons are proportional to the total porosities observed in the samples. A concentration of the porosity of the samples was observed in the mesopore region, with the other porosity distributed among the other scales, corroborating the results obtained from the distributions of relaxation times observed with the NMR analyses.

Absolute Permeability by NMR

Based on the application of existing models in the literature and widely used in industry to estimate permeability, Schlumberger-Doll Research (SDR), Equation (1) Kenyon et al. (1988), and Timur-Coates (TC), Equation (2) Coates et al. (1991), it

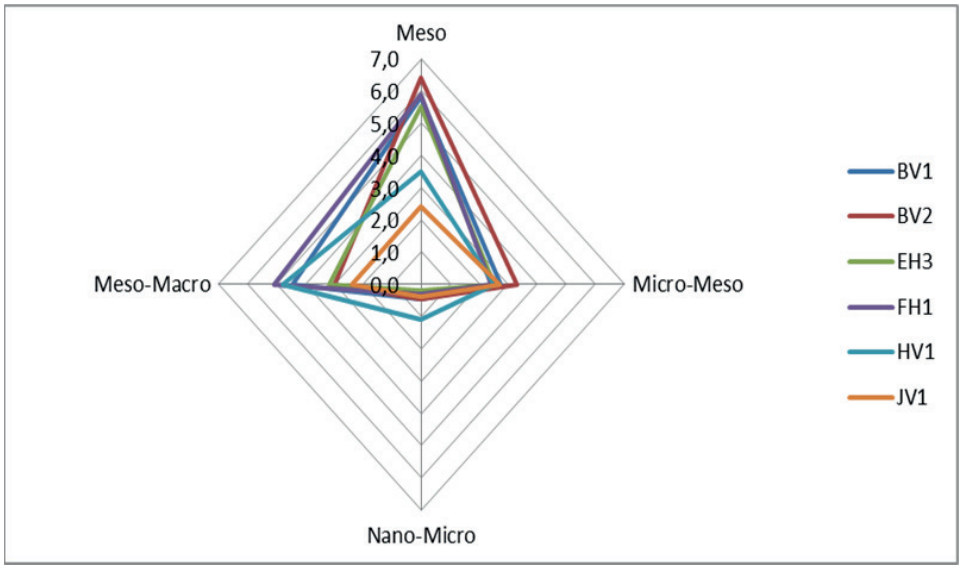

Figure 12. Radar of the distribution of transverse relaxation time (T_2) as a function of the pore scale.

was possible to infer the order of magnitude of the permeability of the samples from the T_2 transverse relaxation spectra.

$$k_{SDR} = a \varnothing^b T_{2gm}^c \quad (1)$$

$$k_{TC} = a \varnothing^b \left(\frac{FFI}{BVI}\right)^c \quad (2)$$

where T_{2gm} is the geometric mean of T_2 and "a," "b," and "c" are the lithological fit coefficients (Table V).

The saturated samples' cutoff at 33 ms (the standard used in sandstones and accepted by the international community) was considered for the FFI/BVI ratio. Although the NMR technique cannot estimate permeability with the same accuracy as direct measurements from routine petrophysics, it is noteworthy that using this mathematical model can significantly assist in decision-making in the exploratory context of possible reserves since it generates results with reasonable accuracy during logging.

Table VI presents the results obtained for the k_{SDR} and k_{TC} models, with the respective values of the correlation coefficients and mean deviations, which were compared with the reference values found in routine petrophysics.

The correlations between the gas permeability values (k_{abs}) and the permeabilities via the SDR (k_{SDR}) and TC (k_{TC}) model by NMR are shown in Figure 13. For the k_{SDR} model, there is a good correlation, with a small deviation from the linear mean of the values. The k_{TC} model showed a better fit, with a higher correlation coefficient (R^2).

The estimated results were coherent and interesting from an analytical point of view since these sandstones have a significant proportion of secondary porosity due to phenomena and diagenetic processes related to the dissolution and replacement of grains. Laboratory characterizations for this type of sandstone sample are practically unprecedented, and it is worth mentioning the work Silva (2014) developed in deposits of the Itararé Group of the Paraná Basin.

Table V. Lithological fit coefficients according to the SDR and TC models.

Model	Lithological Adjustment Coefficients		
	a	b	c
SDR	-7.40	5.80	0.70
TC	-5.33	4.83	-2.13

Table VI. Estimation of permeability by the SDR method and the TC method.

Samples	Permeability (mD)							
	Routine (N_2)	SDR	R^2	RMSE	Routine (N_2)	TC	R^2	RMSE
BV1	2.35	2.11	0.706	0.391	2.35	2.42	0.885	0.152
BV2	1.13	1.36			1.13	0.915		
EH3	0.379	0.581			0.379	0.619		
FH1	2.85	2.06			2.85	3.39		
HV1	1.79	0.538			1.79	1.08		
JV1	0.096	0.097			0.096	0.096		

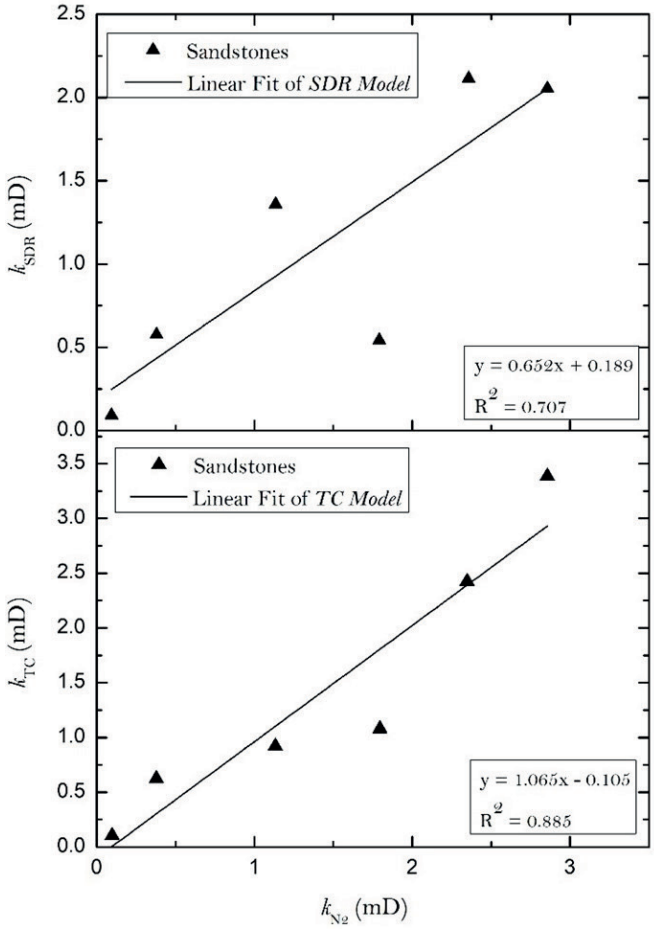

Figure 13. Correlation between the gas permeability (N_2) and that estimated by the k_{SDR} and k_{TC} model.

CONCLUSIONS

It was observed that the results of the petrographic analyses were in agreement with the results obtained by the laboratory evaluations, such as routine petrophysics and NMR based on transversal relaxation (T_2). The estimates of porosity and permeability via NMR, when compared to those of routine petrophysics, showed good correlation, with high coefficients of determination and root mean square errors, where R^2 = 0.957 and RMSE = 0.208 for porosity and R^2 = 0.885 and RMSE = 0.152 for permeability, indicating that, although the samples have undergone a diagenetic process, with the characteristic generation of secondary porosity, the technique was able to infer values lower than one unit of porosity (+/- 1 p.u.), i.e., in a range between 8 to 14%, compared to routine petrophysics. The permeability estimate exhibited predominance for low values (from 0.096 to 2.42 mD), corroborating the high concentration of micro- and mesopores observed in their spectra and the dissolution of the grains observed in the petrographic investigations. In general, the results were consistent, demonstrating the performance of the different integrated or isolated techniques in determining the petrophysical parameters of interest in reservoirs.

Acknowledgments

Special thanks are due to Olívia de Moraes França from the National Observatory for assistance with the laboratory measurements, to the Coordenação de Aperfeiçoamento de Pessoal de Nível Superior (CAPES) for the financial support, to the Department of Stratigraphy and Paleontology, Rio de Janeiro State University – UERJ, for the petrographic analyses and to National Observatory Petrophysics Laboratory - LabPetrON for the petrophysical analyses.

REFERENCES

AMERICAN PETROLEUM INSTITUTE. 1998. Recommended Practice for Core Analysis. API, Washington, p. 236.

BENAVENTE D, DEL CURA MAG, BERNABÉU A & ORDÓÑEZ S. 2001. Quantification of salt weathering in porous stones using an experimental continuous partial immersion method. Eng Geol 59: 313-325. https://doi.org/10.1016/S0013-7952(01)00020-5.

BOCARDI LB, ROSTIROLLA SP, VESELY FF & FRANÇA AB. 2009. Diagenesis, depositional context and burial history of the Rio Bonito Formation, Paraná Basin. Brazilian J Geosci 39: 465-478. https://doi.org/10.25249/0375-7536.2009393465478.

CASAGRANDE J. 2010. Stratigraphic and Structural Analysis of the CBM-bearing Carbonaceous Interval - Early Permian of the Paraná Basin. Master's dissertation, Institute of Geosciences, Federal University of Rio Grande do Sul, Porto Alegre, Brazil, p. 137. (Unpublished).

COATES GR, HARDWICK RCA & ROBERTS D. 1991. The magnetic resonance imaging log characterised by comparison with petrophysical properties and laboratory core data. SPE Annual Technical Conference and Exhibition, Dallas, Texas. Paper SPE-22723-MS. https://doi.org/10.2118/22723-MS.

CRANGANU C, VILLA MA, SARAMET M & ZAKHAROVA N. 2009. Petrophysical characteristics of source and reservoir rocks in the Histria basin, western black sea. J Pet Geol 32: 357-371. https://doi.org/10.1111/j.1747-5457.2009.00455.x.

DOTT RH. 1964. Wacke, greywacke and matrix—What approach to immature sandstone classification? J Sediment Petrol 34: 625-632. https://doi.org/10.1306/74D71109-2B21-11D7-8648000102C1865D.

FOLK RL. 1968. Petrology of Sedimentary Rocks. Hemphill Publishing Company, Austin, Texas, p. 190.

GILES MR & DE BOER RB. 1989. Secondary porosity: creation of enhanced porosities in the subsurface from the dissolution of carbonate cements as a result of cooling formation waters. Mar Pet Geol 6: 261-269. https://doi.org/10.1016/0264-8172(89)90005-6.

GILES MR & MARSHALL JD. 1986. Constraints on the development of secondary porosity in the subsurface: re-evaluation of processes. Mar Pet Geol 3: 243-255. https://doi.org/10.1016/0264-8172(86)90048-6.

GIL VMS & GERALDES CFGC. 1987. Ressonância Magnética Nuclear: Fundamentos, Métodos e Aplicações. Fundação Calouste Gulbenkian, Lisboa.

KENYON WE, DAY PI, STRALEY C & WILLEMSEN JF. 1988. A three-part study of NMR longitudinal relaxation properties of water-saturated sandstones. SPE Form Eval 3: 622-636. https://doi.org/10.2118/15643-PA.

KETZER JM, HOLZ M, MORAD S & AL-AASM IS. 2003. Sequence stratigraphic distribution of diagenetic alterations

in coal-bearing, paralic sandstones: evidence from the Rio Bonito formation (early Permian), southern Brazil. Sedimentology 50: 855-877. https://doi.org/10.1046/j.1365-3091.2003.00586.x.

KLEINBERG RL & JACKSON JA. 2001. An introduction to the history of NMR well logging. Concepts Magn. Reson. 13: 340-342. https://doi.org/10.1002/cmr.1018.

LEVITT MH. 2001. Spin Dynamics: Basic Principles of NMR Spectroscopy. John Wiley & Sons, West Sussex.

LOWDEN BD, PORTER MJ & POWRIE LS. 1998. T_2 relaxation time versus mercury injection capillary pressure: implications for NMR logging and reservoir characterization. European Petroleum Conference, Hague, Netherlands. Paper SPE-50607-MS. https://doi.org/10.2118/50607-MS.

MEDEIROS RA & THOMAS FA. 1973. Facies and depositional environments of the Rio Bonito Formation. Brazilian Congress of Geology, 27, Anais. Aracaju V.3, p. 3-12. http://www.sbgeo.org.br/home/pages/44.

MEIBOOM S & GILL D. 1958. Modified spin-echo method for measuring nuclear relaxation times. Rev Sci Instrum 29: 688-691. https://doi.org/10.1063/1.1716296.

MILANI E & ZALÁN P. 2000. An outline of the geology and petroleum systems of the Paleozoic interior basins of South America. Episodes 22: 199-205. https://doi.org/10.18814/epiiugs/1999/v22i3/007.

MILANI EJ, KINOSHITA EM, DE ARAUJO LM & DA CRUZ CUNHA PR. 1990. Parana Basin: petroleum potential in the depocenter area; Bacia do Parana: possibilidades petroliferas da Calha Central. Geoscience Bulletin - Petrobras 4(1): 21-34.

SCHMIDT V & MCDONALD DA. 1979. Secondary Reservoir Porosity in the Course of Sandstone Diagenesis. AAPG, American Association of Petroleum Geologists, Tulsa, OK, p. 125.

SCHNEIDER RL, MUHLMANN H, TOMMASI E, MEDEIROS RA, DAEMON RF & NOGUEIRA AA. 1974. Stratigraphic review of the Paraná Basin. Brazilian Congress of Geology, Porto Alegre, Brazil, p. 41-66.

SILVA CAM. 2014. Analysis of Petrographic and Petrophysical Properties by Nuclear Magnetic Resonance (NMR) of Sandstones from the Itararé Group - Paraná Basin, Doctoral thesis. Institute of Geosciences. Federal Fluminense University, Rio de Janeiro, Brazil, p. 187.

SILVA LAP. 2011. Characterization of the Mechanical Behavior of Coal from the Rio Bonito Formation, Barro Branco Layer - SC. Master's dissertation, Pontifical Catholic University of Rio de Janeiro, Rio de Janeiro, Brazil, p. 120. (Unpublished).

TIAB D & DONALDSON EC. 2004. Petrophysics - Theory and Practice of Measuring Reservoir Rock and Fluid Transport Properties. Elsevier, New York, p. 920.

ZALÁN PV, WOLFF S, CONCEIÇÃO JCJ, ASTOLFI MAM, VIEIRA IS, APPI VT & ZANOTTO OA. 1987. Tectonics and sedimentation of the Paraná basin. Southern Brazilian Geology Symposium, 3, Curitiba, Brazil. V1: 441-477.

ZHANG Y, XIA P & YU Y. 2000. Review of nuclear magnetic resonance magnet for oil well logging. IEEE Trans Appl Supercond 10: 763-766. https://doi.org/10.1109/77.828343.

How to cite

RAMOS PFO, STAEL GC, AZEREDO RBV, ADE MVB, BERGAMASCHI S, LOURENÇO J & BERMUDEZ SLB. 2024. Petrographic and Petrophysical Characterization of Sandstones from Rio Bonito Formation, Paraná Basin (Southern Brazil). An Acad Bras Cienc 96: e20240365. DOI 10.1590/0001-3765202420240365.

Manuscript received on April 10, 2024;
accepted for publication on August 2, 2024

PAULO FREDERICO O. RAMOS[1]
https://orcid.org/0009-0001-7402-1109

GIOVANNI C. STAEL[2]
https://orcid.org/0000-0003-0162-1119

RODRIGO B.V. AZEREDO[3]
https://orcid.org/0000-0002-0424-2539

MARCUS VINICIUS B. ADE[4]
https://orcid.org/0000-0002-6653-9469

SÉRGIO BERGAMASCHI[4]
https://orcid.org/0000-0001-9395-0520

JUAREZ LOURENÇO[2]
https://orcid.org/0000-0003-0469-0216

SILVIA LORENA B. BERMUDEZ[2]
https://orcid.org/0000-0001-5482-2681

[1]University of Campinas (UNICAMP), Center for Petroleum Studies (CEPETRO), R. Cora Coralina, 350, Cidade Universitária, 13083-896 Campinas, SP, Brazil

[2]National Observatory, Department of Geophysics, R. Gal. José Cristino, 77, 20921-400 Rio de Janeiro, RJ, Brazil

[3]Fluminense Federal University, Institute of Chemistry, Outeiro de São João Batista, s/n, 24020-141 Niterói, RJ, Brazil

[4]State University of Rio de Janeiro, Department of Stratigraphy and Paleontology, Rua São Francisco Xavier, 524, Bloco A, 20550-900 Rio de Janeiro, RJ, Brazil

Correspondence to: **Giovanni Chaves Stael**
E-mail: stael@on.br

Author contributions

All authors contributed to the conception of the work, the analysis and interpretation of data for the work, the manuscript revision, and the reading and approval of the submitted version.